ACS APPLIED MATERIALS & INTERFACES

Research Article

www.acsami.org

Antireflective Coatings with Adjustable Refractive Index and Porosity Synthesized by Micelle-Templated Deposition of MgF_2 Sol Particles

Denis Bernsmeier,[†] Jörg Polte,[‡] Erik Ortel,[†] Thoralf Krahl,[‡] Erhard Kemnitz,[‡] and Ralph Kraehnert*[,†]

[†]Department of Chemistry, Technische Universität Berlin, Straße des 17. Juni 124, 10623 Berlin, Germany

[‡]Department of Chemistry, Humboldt-Universität zu Berlin, Brook-Taylor-Strasse 2, 12489 Berlin, Germany

Supporting Information

ABSTRACT: Minimizing efficiency losses caused by unwanted light reflection at the interface between lenses, optical instruments and solar cells with the surrounding medium requires antireflective coatings with adequate refractive index and coating thickness. We describe a new type of antireflective coating material with easily and independently tailorable refractive index and coating thickness based on the deposition of colloidal MgF_2 nanoparticles. The material synthesis employs micelles of amphiphilic block copolymers as structure directing agent to introduce controlled mesoporosity into MgF_2 film. The coatings thickness can be easily adjusted by the applied coating conditions. The coatings refractive index is determined by the materials porosity, which is controlled by the amount of employed pore template. The refractive index can be precisely tuned between 1.23 and 1.11, i.e., in a range that is not accessible to nonporous inorganic materials. Hence, zero reflectance conditions can be established for a wide range of substrate materials.

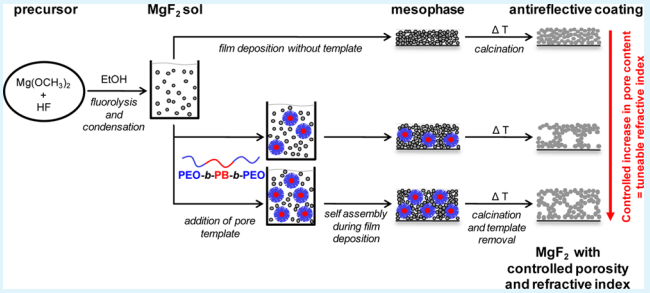

KEYWORDS: *antireflective coating, mesoporous material, micelle, sol–gel, thin film*

1. INTRODUCTION

Transparent optical materials with a refractive index of about 1.5, e.g., typical glasses, reflect about 4.3% of the incident visible light as can be deduced from the Fresnel's laws.[1] Reflection occurs for both material surfaces, i.e., for the incoming and the outgoing light. Eliminating this light reflection would increase significantly the efficiency of optical materials, such as architectural windows, solar panels, or optical lenses.

Zero reflection for a specific wavelength can be obtained by so-called single layer interference if the antireflective coating consists of a transparent material with an optical thickness of one-quarter of the light's wavelength and possesses a refractive index that matches the square root of the substrate's refractive index. For common optical glass materials antireflective coatings with a refractive index of 1.23 are therefore required.[2,3] The effectiveness of a single-layer antireflection coating is limited by the available materials with suitable refractive index: transparent bulk materials with a refractive index of 1.23 do not exist in nature.

Introducing porosity into dense coating layers can be used to decrease their mean refractive index to the desired value.[4] Unfortunately, for the oxide with the lowest refractive index (SiO_2, n = 1.46) about 50% porosity is required for a mean refractive index of 1.23, which decreases drastically the mechanic stability of such porous layers.[5] Falcaro et al. synthesized silica films with about 69% templated porosity and obtained a refractive index of 1.14.[6] Magnesium fluoride (n = 1.38) features one of the lowest refractive indices of all available inorganic materials. Controlling the degree of porosity of MgF_2 would therefore allow to obtain the optimal refractive index for a range of different substrate materials.

Different synthesis routes for the preparation of antireflective coatings have been reported. For oxide materials sputtering processes,[7] evaporation techniques[8] and liquid phase deposition[5] are commonly used, the latter being the most suitable for the synthesis of porous antireflective ("AR") coatings. MgF_2 coatings can be deposited by gas phase techniques,[8] but suffer from poor optical quality due to point defects. Liquid phase deposition of MgF_2 requires suitable precursor solutions. Grosso et al. deposited mixtures of Mg acetate, trifluoroacetic acid, ethanol, and water on Si wafers. The MgF_2 films obtained after a flash thermal treatment at 450 °C were structured by "nanobubbles" and showed a refractive index of 1.09.[9] Also the synthesis of MgF_2 precursor solutions[10] for the sol–gel processing of MgF_2 thin films[11,12] has been reported. Unfortunately, the precursors are often very reactive and thus corrode typical substrates.

MgF_2 particles could be ideal precursors because of their high phase purity. Murata et al. prepared colloidal MgF_2 and casted films with textural porosity via spin-coating and subsequent drying.[13,14] The films showed a refractive index of 1.42. Treating the sol prior to deposition in an autoclave at 140°

Received: April 4, 2014
Accepted: October 21, 2014
Published: November 5, 2014

Scheme 1. Schematic Description of the Developed Synthesis Method for Magnesium Fluoride Films with Porosity-Controlled Refractive Index and Adjustable Thickness[a]

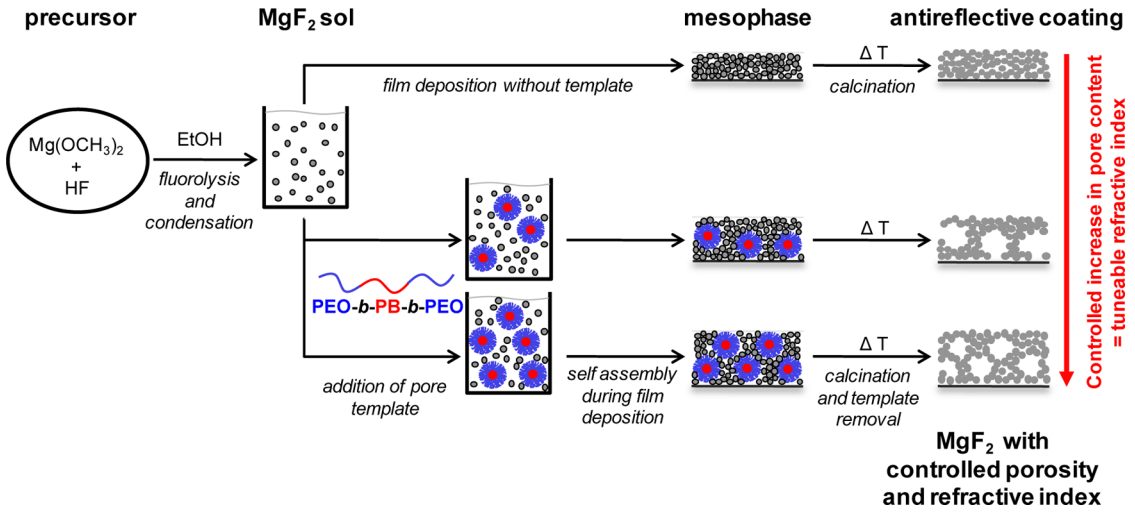

[a]MgF_2 sols are synthesized and then codeposited with different quantities of block-copolymer PEO−PB−PEO. The polymer acts as pore template. After thermal treatment porous MgF_2 films are obtained. The amount of template controls the obtained porosity and refractive index. Higher withdrawal speeds from the solution produce thicker MgF_2 films.

increased the particle size and changed the films refractive index to 1.29.

The deposition of coatings with ordered and template-controlled porosity from colloidal particles has been reported recently for titania by Brezesinski et al.,[15] Szeifert et al.,[16] and Ortel et al.[17] In these approaches, colloidal solutions of oxide nanoparticles are deposited along with micelles of amphiphilic block copolymers forming ordered mesophases. Subsequent removal of the template polymers by calcination yields oxides with a high degree of porosity resulting in specific surface areas up to 300 m^2/g.

The present contribution describes a new method for the synthesis of antireflective MgF_2 layers with almost 100% optical transparency and easily tailorable refractive index. The approach is illustrated in Scheme 1. In this approach, MgF_2 sols are deposited as nanocrystalline building blocks along with structure-directing block copolymers to construct mesostructured films via dip-coating. Thermal removal of the polymer yields transparent mesoporous films. The porosity of deposited films can be controlled by variation of the content of polymer in the dip-coating mixture, which enables a direct adjustment of the refractive index of the MgF_2 coatings.

The following sections describe the synthesis of the precursor sol, the method of film deposition and the successful synthesis of MgF_2 films with micelle-controlled porosity. Thereafter, the effects of template concentration, coating conditions and calcination temperature on the film morphology are discussed. Finally, it is demonstrated that the refractive index (measured by ellipsometry) can be adjusted reproducibly between 1.11 and 1.23 independent of the respective film thickness.

2. EXPERIMENTAL SECTION

Chemicals. The polymer template PEO_{184}−PB_{213}−PEO_{184}, a poly(ethylene oxide)-*b*-poly(butadiene)-*b*-poly(ethylene oxide) block copolymer (containing 18 700 g/mol PEO and 10 000 g/mol PB) was synthesized by Polymer Service Merseburg GmbH following a procedure described in.[17]

All chemicals for the synthesis of magnesium fluoride were used as received without drying or further processing. For better handling and dosing the HF solution used for these experiments was prepared by condensation of HF (Solvay Fluor GmbH, Hannover) in ethanol. Magnesium turnings (Aldrich, 99.98%) were used as supplied.

Synthesis of MgF_2 Sol. Magnesium methoxide was prepared by dissolution of Mg turnings (1.50 g, 61.7 mmol) in 247 mL dry MeOH to give a 0.25 molar $Mg(OMe)_2$ solution. For fluorolysis of $Mg(OMe)_2$, a stoichiometric amount of alcoholic HF (concentrations between 7.5 and 9.3 M) was added to the alkoxide solution within 5 min under vigorous stirring to give the desired product.[18] The synthesis provides clear MgF_2 sols[19] (see the Supporting Information, Figure S1a) suitable for processing in liquid deposition techniques like spin-coating[20] or dip-coating.[21,22]

$$Mg(OCH_3)_2 + 2HF \rightarrow \text{nano-}MgF_2 + 2CH_3OH \quad (1)$$

^{19}F NMR spectra (see the Supporting Information, Figure S1) of the sols indicate the formation of pure MgF_2 with typical very broad signals at around −198 ppm, which is attributed to the fluorine in the rutile structure of magnesium fluoride. A second peak at ∼180 ppm can be attributed to $MgF_{6-x}O_x$ species.[23] XRD-diffraction evidenced the presence of highly distorted nearly amorphous MgF_2.[23] The mean hydrodynamic diameter (see the Supporting Information, Figure S1) of the as-synthesized MgF_2 particles was determined to 4 nm by dynamic light scattering (DLS). The employed MgF_2 sol has a concentration of 0.54 mol/L. The sols are stable for at least 6 months.[23]

Synthesis of Porous MgF_2 Coatings. Before film deposition silicon wafers were cleaned with pure ethanol and calcined for 2 h in air at 600 °C. Silica plates were cleaned with pure ethanol. The template polymer PEO_{213}−PB_{184}−PEO_{213}[17] was dispersed in ethanol and mixed with the MgF_2 sol until a clear suspension was obtained. Films were deposited via dip-coating at 25 °C and 40% relative humidity and dried for 3 min at these conditions. Thereafter, films were transferred into a preheated muffle furnace, calcined for 20 min in air, removed from the furnace, and cooled down naturally to room temperature.

Material Characterization. Liquid phase ^{19}F NMR ($\nu_{Larmor}(^{19}F)$ = 282.4 MHz) of the sol was recorded on a Bruker AVANCE II 300. Dynamic light scattering (DLS) experiments were performed using a Zetasizer Nano ZS (Malvern Instruments, Worcestershire, UK).

Film samples were scraped off the substrates, collected on a carbon-coated copper grid and then studied by TEM using a FEI Tecnai G 2

dx.doi.org/10.1021/am5052685 | ACS Appl. Mater. Interfaces 2014, 6, 19559−19565

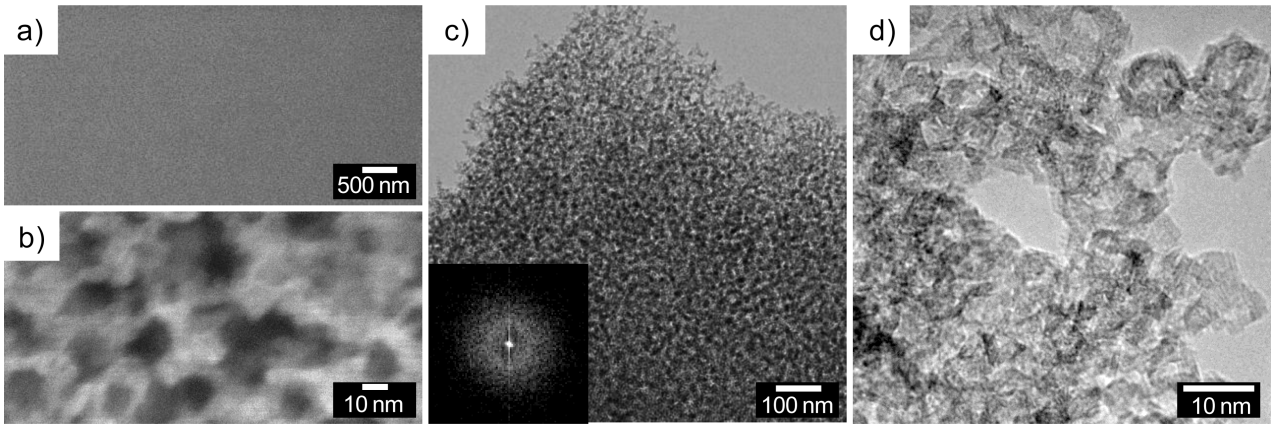

Figure 1. SEM and TEM analysis of the morphology of a micelle-templated MgF_2 film (4.0 wt % PEO−PB-PEO, calcination at 400 °C). (a) SEM image (top-view) in low magnification proofs homogeneity of the film, (b) SEM image (top-view) shows template mesoporosity, (c) TEM image and corresponding FFT inset confirm porosity and pore order throughout the material. (d) HRTEM: the pore walls are composed of particles of about 5 nm size.

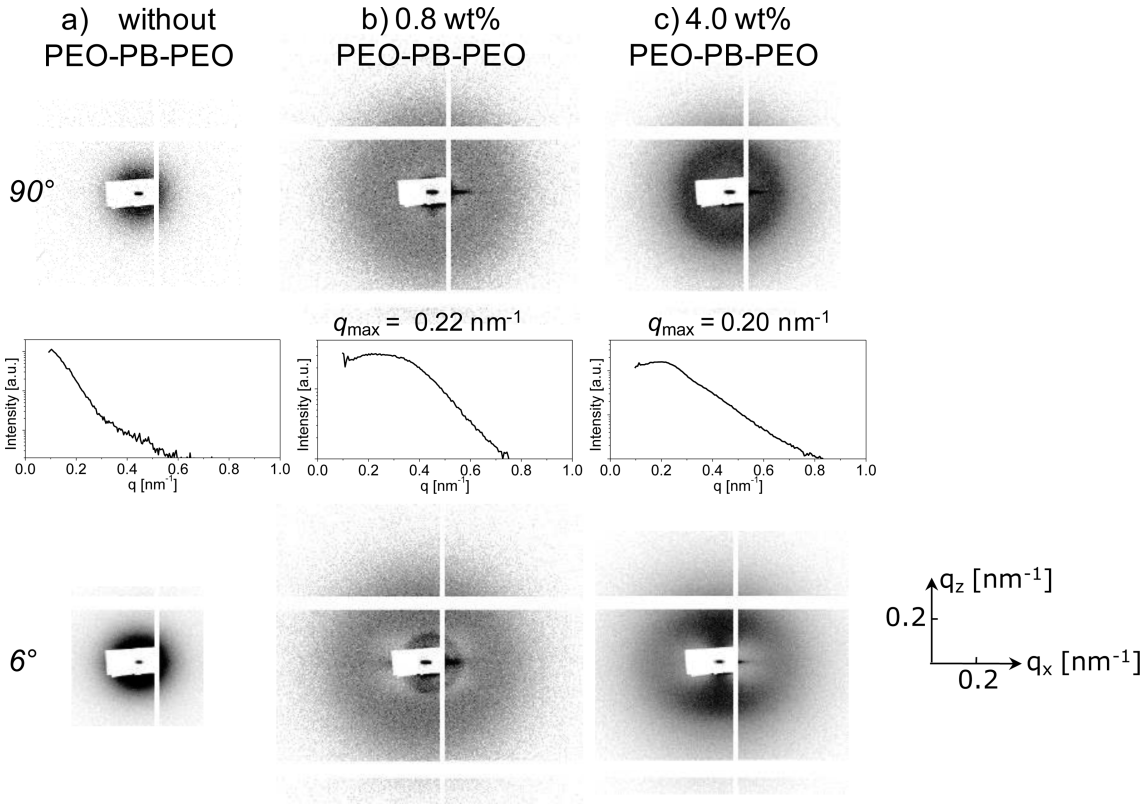

Figure 2. 2D-SAXS patterns of calcined MgF_2 films (T_{calc} = 500 °C) with varied template concentration (increasing from left to right): a) without pore template, (b) 0.8 wt % PEO−PB-PEO, (c) 4.0 wt % PEO−PB-PEO in the dip-coating mixture. SAXS was recorded in transmission with beam incident angles of 90° (upper row) with corresponding 1D-SAXS patterns (middle row) and 6° (bottom row) relative to the substrate surface.

20 S-TWIN instrument operated at 200 kV. SEM images were recorded on a JEOL 7401F instrument at 10 kV. ImageJ Version 1.45s was employed for quantitative analysis and for fast Fourier transformation.

Kr adsorption isotherms were measured at 77 K with a Quantachrome Autosorb-1-C. The film samples were degassed in vacuum at 150 °C for 2 h prior to physisorption. Surface area was calculated using the method of Brunauer−Emmett−Teller (BET).

2D SAXS patterns were recorded at HASYLAB B1 beamline at DESY Hamburg with a PILATUS 1 M detector at a sample to detector distance of 3583 mm and a calibrated energy of 16026 eV. XRD was measured on a Bruker D8 Advance (Cu K_α radiation) with gracing incident beam (1°). Reflections were assigned using PDF MaintEx library Version 9.0.133. The average crystallite size was calculated applying the Scherrer equation.

The ellipsometric measurements were carried out on MgF_2 coated Si wafers using a M2000DI (J. A. Woollam) ellipsometer. Each sample was measured at angles of incidence of 65, 70, and 75° in a spectral range between 190 and 1700 nm. For intrasample homogeneity studies, the layers were measured at 13 different points as described in.[20] The ellipsometric data were analyzed using the WVASE32 software.

The film porosity was calculated in analogy to[24,25] based on analysis of the mass depth obtained via StrataGem film analysis software (v

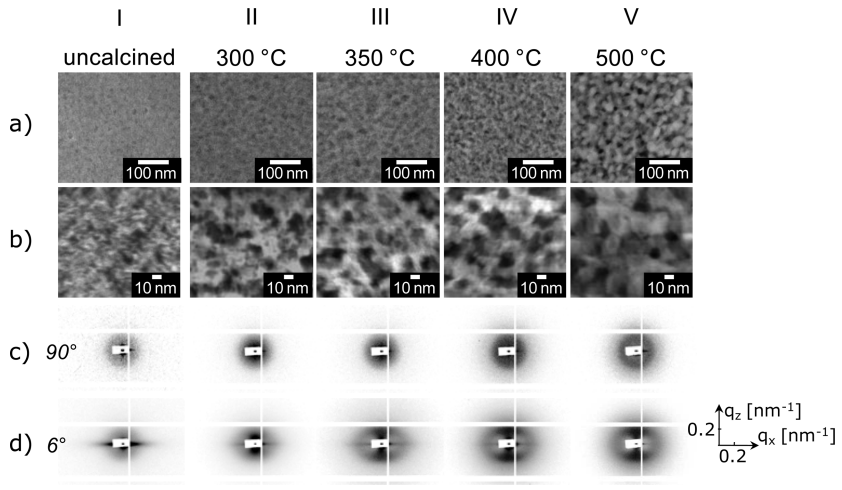

Figure 3. Influence of calcination temperature on film morphology ((a, b) SEM) and pore order ((c, d) SAXS) of micelle-templated MgF_2 films (4.0 wt % PEO−PB-PEO). Top-view SEM mages at (a) 100k and (b) 300k magnification. 2D SAXS recorded in transmission with beam incident angles of (c) 90° and (d) 6° relative to the substrate surface. Samples: (I) uncalcined and calcined at (II) 300, (III) 350, (IV) 400, and (V) 500 °C.

2.6.0) using EDX spectra measured on a Thermo Scientific NORAN System in a Zeiss Supra 40 microscope with a Schottky field emitter.

UV/vis spectra were recorded on a AvaSpec-2048TEC-2 spectrometer equipped with a deuterium halogen light source (Avantes, Broomfield, USA) using a CUV-10−2 cell for transmittance measurements and a FCR-7UV400−2-ME-HTX probe for reflection measurements.

3. RESULTS AND DISCUSSION

Morphology of Templated MgF_2 Coatings. SEM and TEM analysis of a MgF_2 film prepared with a polymer concentration of 4.0 wt % and calcined at 400 °C is shown in Figure 1. The top-view SEM images (Figure 1a, b) indicate the homogeneity of the film and the abundant presence of mesopores with a diameter of ca. 14 nm. Bright-field TEM images of film samples (Figure 1c) confirm mesoporosity throughout the material. The corresponding FFT (inset in Figure 1c) shows an isotropic ring, which indicates that mesopores are locally ordered with a periodic distance of approximately 30 nm. High resolution micrographs of the same sample (HRTEM) (Figure 1d) show pores with ca. 12 nm diameter and pore walls composed of smaller particles. The observed pore sizes and pore distances are similar to typical mesoporous structures of sol−gel-derived oxide films (TiO_2;[17] MgO;[26] ZnO, Co_3O_4[27]) and nanoparticle-derived mesoporous titania (17 nm)[17] templated by the same block copolymer PEO_{213}−PB_{184}−PEO_{213}. The results suggest that micelle templates are incorporated into the deposited mesophase and removed during subsequent calcinations resulting in the desired regular open mesoporous structure.

The presence of pore ordering in the templated and untemplated films was investigated by small-angle X-ray scattering (SAXS) in transmission configuration on films deposited on thin Si-wafers (50 μm). Figure 2 depicts the corresponding 2D-SAXS patterns of films recorded at β = 90° (upper row) with corresponding 1D-SAXS patterns (middle row) and β = 6° (lower row) between incident beam and film surface. Without polymer addition (a) the measurements show no scattering from periodic structures at characteristic distances. In contrast, a broad diffraction ring can be observed for a sample synthesized with 0.8 wt % of template polymer (b). Moreover, a polymer concentration of 4.0 wt % (c) produces a film with a clear isotropic ring for SAXS recorded at β = 90° and an ellipsoidal diffraction pattern for β = 6°. The diffraction ring confirms local ordering parallel to the substrate surface. In line with these observations, the 1D-SAXS pattern (middle row) shows no diffraction peak from the film made without polymer (a), a broad peak with a maximum at a q value of 0.22 nm^{-1} for the film made with 0.8 wt % polymer (b) and a more distinct peak at q_{max} = 0.20 nm^{-1} for the film made with 4.0 wt % polymer (c). The q_{max} corresponds to a periodicity of ca. 32 nm. This value agrees well with the periodic distance observed in FFT analysis of TEM images (30 nm, Figure 1c). Such ellipsoidal patterns are typically observed for micelle-templated oxide films and commonly attributed to film and pore shrinkage perpendicular to the substrate. The measured q value and pore shrinkage are comparable to other porous metal oxide films templated with the same amphiphilic block copolymer[26,28] analyzed by SAXS in transmission with similar beam incident angles. A direct comparison with mesoporous films assembled from nanocrystalline TiO_2 building blocks[17] indicates that the mesoporous MgF_2 has a lower degree of pore ordering. The broad and weak diffraction rings observed for templated MgF_2 suggest that the extent of pore ordering is very weak, in particular when compared with oxide films prepared from molecular precursors. The absence of diffraction patterns in case of the untemplated MgF_2 film (Figure 2a) confirms that the formation of locally ordered mesopores occurs only in the presence of the polymer template.

Calcination represents the final synthesis step and removes organic templates, stabilizer and solvents from the deposited film. To study the influence of thermal treatments on the film morphology, template MgF_2 films were analyzed by SEM and SAXS prior to calcination and after calcination at 300, 350, 400, and 500 °C. Figure 3 displays corresponding SEM images in (a) low and (b) high magnification and 2D-SAXS patterns of films recorded at (c) β = 90° and at (d) β = 6°.

SEM images (Figure 3Ia, Ib) recorded prior to calcinations show weak contrast but already suggest a structure made of sol particles as well as pores between the particles. The SAXS measurements (Ic and Id) reveal no clear scattering from periodic structures yet. SEM images (IIa and IIb) of a film calcined at 300 °C are richer in contrast than the noncalcined film and the high magnification image (IIb) reveals a porous

dx.doi.org/10.1021/am5052685 | ACS Appl. Mater. Interfaces 2014, 6, 19559−19565

structure. SAXS analysis (IIc and IId) shows no scattering from periodic structures. After calcination at 350 °C (IIIa and IIIb) and at 400 °C (IVa and IVb), mesopore walls can be clearly distinguished by SEM. The SAXS patterns of films calcined at 350 and 400 °C recorded at tilted angles (IIId and IVd) start to reveal an ellipsoidal ring confirming locally ordered pores which are contracted normal to the surface. Films calcined at 500 °C (Va and Vb) exhibit larger sol particles arranged around mesopores. The SAXS pattern collected at 90° incident angle (Vc) displays an isotropic ring, whereas the analysis on the tilted sample shows an ellipsoidal ring.

The observation of locally ordered pore structures above 300 °C is consistent with thermogravimetric analysis of the employed template polymer. The template typically decomposes between 270 and 425 °C, giving rise to the formation of open mesopores.[26] Complementary thermal analysis (DTA) of the MgF_2 sol, published in,[29] shows a mass loss between 100 to 350 °C because of a loss of water and the complete removal of OH surface groups at 500 °C. This complete removal of other species seems to increase the difference in electron density between pores and pore walls, hence samples calcined at 500 °C show the highest contrast in SAXS analysis (Figure 3Vc). Calcination at 500 °C therefore provides MgF_2 films with locally ordered mesopores and assures the removal of all organic substances and solvents.

To study the influence of thermal treatment on the film thickness, we recorded cross-section SEM images of films after calcination at different temperatures (see the Supporting Information, Figure S2). All films exhibit approximately the same film thickness as the uncalcined (dried) sample. Hence, films do not shrink significantly during calcination.

The influence of the template polymer on material crystallinity was analyzed by XRD for films synthesized with different polymer content prior to calcination and after calcination at 500 °C (Figure 4). All calcined films show reflections that clearly identify crystalline MgF_2 because of the appearance of reflections at 2 Theta angles of 27.28° (110), 35.20° (101), 40.40° (111), 43.76° (210), 53.51° (211), and 56.27° (220) [PDF: 41−1443]. (Note that the reflection at 17 °C in Figure 4a results from a silicon oxide, i.e., the oxidized surface of the Si substrate, not the deposited film.) Crystallite sizes estimated from the broadening of the measured MgF_2 reflections using Scherrer equation amount to ca. 12 nm (no template), 14 nm (0.8 wt %), and 11 nm (4.0 wt %). A noncalcined film (a) measured as a reference shows only faint reflections, indicative of much lower crystallinity. Hence, calcination at 500 °C produces crystalline MgF_2 films. The addition of template has no significant influence on the final crystallite size.

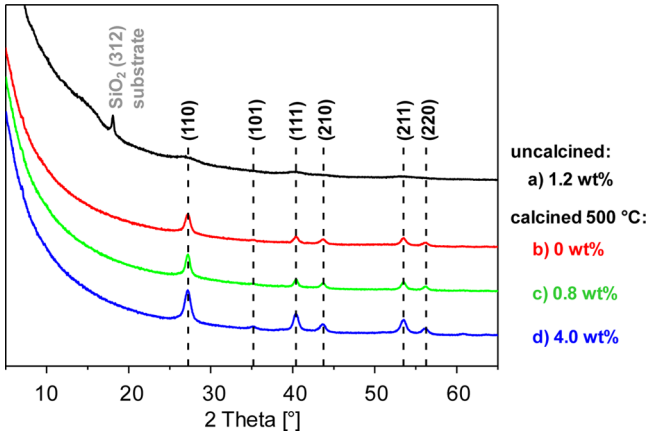

Figure 4. Influence of pore template and calcination at 500 °C on crystallinity of MgF_2 films (a) as-deposited film with 1.2 wt % PEO−PB-PEO, (b) calcined film without PEO−PB-PEO, (c) calcined film with 0.8 wt % PEO−PB-PEO, and (d) calcined film with 4.0 wt % PEO−PB-PEO. Dashed lines indicate the reflection positions for tetragonal MgF_2. [*P*42/*mnm*, PDF No. 00−041−1443] The Peak at 17° originates from the SiO_2 layer of the substrate. [PDF No. 00−051−1381].

The influence of the template on the films surface area was studied by Kr physisorption performed on MgF_2 films calcined at 500 °C and prepared with different template content. The BET surface area (normalized to a film thickness of 100 nm) decreases from 14.3 m^2 per m^2 film surface for a film made without template polymer to 14.0 m^2/m^2 for a film made from a dip-coating mixture with 0.8 wt % template and 12.2 m^2/m^2 for a sample made with 4.0 wt % polymer (see the Supporting Information, Figure S3). Hence, the surface area decreases with increasing polymer content.

This result is consistent with the observed film microstructure. The film prepared without template is dominated by textural porosity formed in-between the deposited sol particles. Addition of the template creates additional mesopores. Hence, the same film volume contains more mesopores, whereas a smaller amount of pore walls and textural microporosity can be accommodated, which leads to a decrease in surface area per film volume.

Optical Properties As a Function of Film Thickness and Mesopore Content. The aim of the present study was a controlled variation of the refractive index and thickness of antireflective MgF_2 coatings. To demonstrate that the porosity tuning by templating induced controlled changes of the refractive index MgF_2 layers with different porosity were analyzed by ellipsometry. Films prepared without template polymer, with 0.8 wt % and with 4.0 wt % polymer were analyzed after calcination at 500 °C. Moreover, each film composition was synthesized with three different withdrawal speeds *U* (100 mm/min (□), 200 mm/min (◇), and 300 mm/min (Δ)) to vary the film thickness and test for reproducibility of the analysis of the refractive index. Evaluation of the ellipsometry data provided the film thickness and the refractive index of layers coated onto silicon substrates.

Figure 5 presents the obtained thickness *d* (a) and refractive index *n* (b) as a function of polymer concentration. The coating's thickness gradually increases with increasing withdrawal rate and increasing polymer content (Figure 5a) from ca. 100 nm to ca. 700 nm. This behavior is in agreement with the historical Landau-Levich's equation[30] and more adapted models for evaporating systems,[31,32] which predict that the higher viscosity caused by increased polymer content in the coating solution and faster substrate withdrawal from the solution should result in thicker films. The thickness values obtained from ellipsometry are in good agreement with respective values obtained from cross-section SEM measurements (see Supporting Information, Figure S4) except for the thickest film (300 mm/min (Δ) with the highest polymer content (4.0 wt % mass fraction PEO−PB-PEO). The deviation can be attributed to limitation in the accuracy of the fitting model for the ellipsometric measurement of thick films.

Nontemplated MgF_2 coatings exhibit a refractive index *n* of approximately 1.23 (Figure 5b, c = 0 wt %). The value is clearly

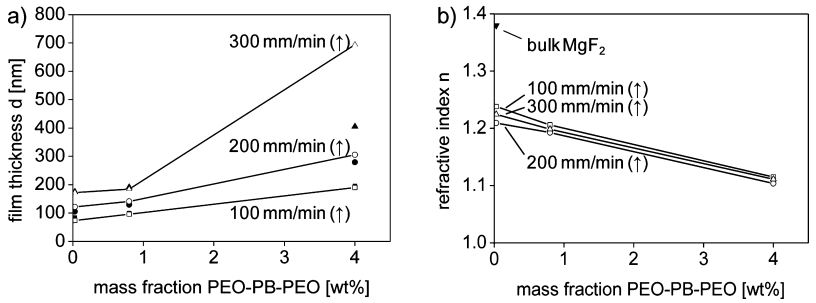

Figure 5. Controlled variation of (a) film thickness and (b) refractive index of micelle-templated MgF_2 coatings. (a) Film thickness as a function of the mass fraction of template in the dip-coating solution and withdrawal rate during dip-coating (open symbols, ellipsometry; filled symbols, from cross-section SEM). (b) Corresponding refractive index (from ellipsometry).

Table 1. Porosity and Refractive Indeces of MgF_2 Films

	film thickness				porosity		refractive index n	
mass fraction of polymer in dip coating solution (wt %)	by SEM (nm)	by elippsometry (nm)	mass depth by EDX/ StrataGem ($\mu g/cm^2$)	density ρ from mass depth (g/cm^3)	from n (%)	from ρ (%)	from porosity (ρ)	by ellipsometry
0	175	172	29.7	1.70	40	46	1.21	1.22
0.8	191	184	29.2	1.53	47	51	1.19	1.20
4.0	405	694	33.6	0.83	71	73	1.10	1.11

below the bulk refractive index of MgF_2 (n = 1.38), which can be explained by the observed textural porosity in between the deposited MgF_2 particles. The porosity of the film therefore amounts to approximately 40% (assuming a refractive index of bulk MgF_2 for the pore walls and n = 1.00 for the pores).[9] The addition of polymer template induces a further decrease in refractive index to n = 1.20 (0.8 wt %) and n = 1.11 (4.0 wt %) (Figure 5b) indicating a direct correlation between the porosity controlled by the template and the overall refractive index of the porous film. From the refractive index a porosity of about ca. 47% (0.8 wt % template) and 71% (4.0 wt % template) can be estimated. Moreover, the observed n values are almost independent of the obtained film thickness, proving the accuracy and reproducibility of the developed synthesis method. Hence, the presented synthesis method enables the precise adjustment of the refractive index of antireflective MgF_2 coatings between 1.11 and 1.23 with the additional benefit of independent control of the film's thickness.

The obtained porosity values can be compared to porosity values derived from mass depth determination by StrataGem software of EDX measurements. Employing film thicknesses measured from cross-section SEM analyses allows the calculation of film volume and film density. Assuming the bulk porosity of MgF_2 for the pore walls (3.13 g/cm^3) allows an estimate of the film's porosity. Table 1 summarizes the specifications for 0, 0.8, and 4.0 wt % mass fraction of polymer in the dip-coating solution. Porosity values obtained from mass depth measurements amount to 46, 51,and 73%, respectively. The porosity shows similar values as estimated from the films refractive indices as derived from ellipsometry (40, 47,and 71%). Moreover, also the increase in porosity with increasing polymer content in the dip-coating solution is well-reproduced.

The antireflective effect of MgF_2 coatings with templated porosity was confirmed by UV−vis spectroscopy recorded in transmission and in reflection mode on uncoated and coated SiO_2 substrates (see the Supporting Information, Figure S5). The uncoated substrates transmit about 94% of the light between 500 and 800 nm wavelength. This value increases to about 99% transmission when the MgF_2 coatings are present, clearly indicating their antireflective properties. UV−vis reflectance spectroscopy recorded perpendicular to the films surface plane (see the Supporting Information, Figure S5) shows a reduced reflectance for MgF_2 coatings in respect to uncoated silica substrates. Compared to the uncoated silica a reflectance as low as about 2% is achieved for films that have a refractive index which matches the square root of the substrate's refractive index n of $(1.46)^{1/2}$ = 1.21. The lowest reflectance is observed for a wavelength of about 4 times the films thickness. A film with a lower refractive index n of 1.11 shows a slightly higher reflectance of 9%.

4. CONCLUSION

Homogeneous, crack-free MgF_2 films can be obtained by codeposition of colloidal MgF_2 particles and micellar pore templates via dip-coating and subsequent calcination. The resulting films are transparent, macroscopically homogeneous and can be deposited on Si-wafer as well as on SiO_2-glass substrates. The employed triblock copolymer PEO_{213}−PB_{184}−PEO_{213} acts as a structure directing agent and produces locally ordered mesopores of ca. 12 nm in diameter inside the film with periodic distances of ca. 32 nm. Ellipsometry proves that the refractive index is controlled by the templated mesoporosity of the layer. The refractive index n can be tuned between 1.11 and 1.23 by the amount of polymer added to the deposition solution. Moreover, the film thickness can be varied independent of the refractive index by variation of the withdrawal rate during dip-coating. Hence, high-quality antireflective coatings can be reproducibly synthesized with unprecedented control over film thickness and refractive index.

■ ASSOCIATED CONTENT

Supporting Information

Additional information about the employed MgF_2 sol, cross-section SEM images, Kr-BET analyses of films, and UV/vis measurements. This material is available free of charge via the Internet at http://pubs.acs.org.

AUTHOR INFORMATION

Corresponding Author

*E-mail: ralph.kraehnert@tu-berlin.de.

Notes

The authors declare no competing financial interest.

ACKNOWLEDGMENTS

Portions of this research were conducted on beamline B1 at light sources DORIS III and PETRA III at DESY, a member of the Helmholtz Association (HGF). We thank Olaf Kahle for ellipsometric measurements at Fraunhofer PYCO, Ulla Vainio for SAXS analysis and Benjamin Paul for UV−vis analysis. D.B. and R.K. gratefully acknowledge financial support from BMBF (FKZ 03EK3009). J.P. acknowledges generous funding by the Deutsche Forschungs-gemeinschaft within Project PO 17441-1. ZELMI at TU Berlin is acknowledged for TEM access.

REFERENCES

(1) Boutry, G. A. Augustin Fresnel: His Time, Life and Work 1788−1827. *Sci. Prog.* **1948**, *36*, 587−604.

(2) Wongcharee, K.; Brungs, M.; Chaplin, R.; Hong, Y. J.; Pillar, R.; Sizgek, E. Sol-Gel Processing by Aging and Pore Creator Addition for Porous Silica Antireflective Coatings. *J. Sol−Gel Sci. Technol.* **2002**, *25*, 215−221.

(3) Prene, P.; Priotton, J. J.; Beaurain, L.; Belleville, P. Preparation of a Sol-Gel Broadband Antireflective and Scratch-resistant Coating for Amplifier Blastshields of the French Laser LIL. *J. Sol−Gel Sci. Technol.* **2000**, *19*, 533−537.

(4) Faustini, M.; Nicole, L.; Boissière, C.; Innocenzi, P.; Sanchez, C.; Grosso, D. Hydrophobic, Antireflective, Self-Cleaning, and Antifogging Sol−Gel Coatings: An Example of Multifunctional Nanostructured Materials for Photovoltaic Cells. *Chem. Mater.* **2010**, *22*, 4406−4413.

(5) Glaubitt, W.; Lobmann, P. Antireflective Coatings Prepared by Sol−Gel Processing: Principles and Applications. *J. Eur. Ceram. Soc.* **2012**, *32*, 2995−2999.

(6) Falcaro, P.; Malfatti, L.; Kidchob, T.; Giannini, G.; Falqui, A.; Casula, M. F.; Amenitsch, H.; Marmiroli, B.; Grenci, G.; Innocenzi, P. Hierarchical Porous Silica Films with Ultralow Refractive Index. *Chem. Mater.* **2009**, *21*, 2055−2061.

(7) Martinu, L.; Biederman, H.; Holland, L. Thin-Films Prepared by Sputtering MgF2 in an Rf Planar Magnetron. *Vacuum* **1985**, *35*, 531−535.

(8) Jacob, D.; Peiro, F.; Quesnel, E.; Ristau, D. Microstructure and Composition of MgF2 Optical Coatings Grown on Si Substrate by PVD and IBS Processes. *Thin Solid Films* **2000**, *360*, 133−138.

(9) Grosso, D.; Boissiere, C.; Sanchez, C. Ultralow-Dielectric-Constant Optical Thin Films Built from Magnesium Oxyfluoride Vesicle-Like Hollow Nanoparticles. *Nat. Mater.* **2007**, *6*, 572−575.

(10) Fujihara, S.; Tada, M.; Kimura, T. Preparation and Characterization of MgF2 Thin Film by a Trifluoroacetic Acid Method. *Thin Solid Films* **1997**, *304*, 252−255.

(11) Joosten, P. H.; Heller, P.; Nabben, H. J. P.; Vanhal, H. A. M.; Popma, T. J. A.; Haisma, J. Optical Thin-Layers of MgF2 Produced by Decomposition of Organic Magnesium-Fluoro Compounds. *Appl. Opt.* **1985**, *24*, 2674−2678.

(12) Bass, J. D.; Boissiere, C.; Nicole, L.; Grosso, D.; Sanchez, C. Thermally Induced Porosity in CSD MgF_2-Based Optical Coatings: An Easy Method to Tune the Refractive Index. *Chem. Mater.* **2008**, *20*, 5550−5556.

(13) Murata, T.; Ishizawa, H.; Motoyama, I.; Tanaka, A. Preparation of High-Performance Optical Coatings with Fluoride Nanoparticle Films Made from Autoclaved Sols. *Appl. Opt.* **2006**, *45*, 1465−1468.

(14) Murata, T.; Ishizawa, H.; Tanaka, A. Investigation of MgF_2 Optical Thin Films with Ultralow Refractive Indices Prepared from Autoclaved Sols. *Appl. Opt.* **2008**, *47*, C246−C250.

(15) Brezesinski, T.; Wang, J.; Polleux, J.; Dunn, B.; Tolbert, S. H. Templated Nanocrystal-Based Porous TiO_2 Films for Next-Generation Electrochemical Capacitors. *J. Am. Chem. Soc.* **2009**, *131*, 1802−1809.

(16) Szeifert, J. M.; Feckl, J. M.; Fattakhova-Rohlfing, D.; Liu, Y. J.; Kalousek, V.; Rathousky, J.; Bein, T. Ultrasmall Titania Nanocrystals and Their Direct Assembly into Mesoporous Structures Showing Fast Lithium Insertion. *J. Am. Chem. Soc.* **2010**, *132*, 12605−12611.

(17) Ortel, E.; Fischer, A.; Chuenchom, L.; Polte, J.; Emmerling, F.; Smarsly, B.; Kraehnert, R. New Triblock Copolymer Templates, PEO-PB-PEO, for the Synthesis of Titania Films with Controlled Mesopore Size, Wall Thickness, and Bimodal Porosity. *Small* **2012**, *8*, 298−309.

(18) Kemnitz, E.; Gross, U.; Rudiger, S.; Shekar, C. S. Amorphous Metal Fluorides with Extraordinary High Surface Areas. *Angew. Chem., Int. Ed.* **2003**, *42*, 4251−4254.

(19) Ruediger, S.; Kemnitz, E. The Fluorolytic Sol−Gel Route to Metal Fluorides - a Versatile Process Opening a Variety of Application Fields. *Dalton Trans.* **2008**, 1117−1127.

(20) Kruger, H.; Kemnitz, E.; Hertwig, A.; Beck, U. Moderate Temperature Sol-Gel Deposition of Magnesium Fluoride Films for Optical UV-Applications: A Study on Homogeneity Using Spectroscopic Ellipsometry. *Phys. Status Solidi A* **2008**, *205*, 821−824.

(21) Kruger, H.; Hertwig, A.; Beck, U.; Kemnitz, E. Low Temperature Sol−Gel Metal Oxide and Fluoride Layer Stacks for Optical Applications. *Thin Solid Films* **2010**, *518*, 6080−6086.

(22) Noack, J.; Scheurell, K.; Kemnitz, E.; Garcia-Juan, P.; Rau, H.; Lacroix, M.; Eicher, J.; Lintner, B.; Sontheimer, T.; Hofmann, T.; Hegmann, J.; Jahn, R.; Lobmann, P. MgF_2 Antireflective Coatings by Sol−Gel Processing: Film Preparation and Thermal Densification. *J. Mater. Chem.* **2012**, *22*, 18535−18541.

(23) Noack, J.; Emmerling, F.; Kirmse, H.; Kemnitz, E. Sols of Nanosized Magnesium Fluoride: Formation and Stabilisation of Nanoparticles. *J. Mater. Chem.* **2011**, *21*, 15015−15021.

(24) Novák, V.; Ortel, E.; Winter, B.; Butz, B.; Paul, B.; Kočí, P.; Marek, M.; Spiecker, E.; Kraehnert, R. Prototyping of Catalyst Pore-Systems by a Combined Synthetic, Analytical and Computational Approach: Application to Mesoporous TiO_2. *Chem. Eng. J.* **2014**, *248*, 49−62.

(25) Bernsmeier, D.; Ortel, E.; Polte, J.; Eckhardt, B.; Nowag, S.; Haag, R.; Kraehnert, R. Versatile Control over Size and Spacing of Small Mesopores in Metal Oxide Films and Catalytic Coatings via Templating with Hyperbranched Core-Multishell Polymers. *J. Mater. Chem. A* **2014**, *2*, 13075−13082.

(26) Eckhardt, B.; Ortel, E.; Polte, J.; Bernsmeier, D.; Gorke, O.; Strasser, P.; Kraehnert, R. Micelle-Templated Mesoporous Films of Magnesium Carbonate and Magnesium Oxide. *Adv. Mater.* **2012**, *24*, 3115−3119.

(27) Eckhardt, B.; Ortel, E.; Bernsmeier, D.; Polte, J.; Strasser, P.; Vainio, U.; Emmerling, F.; Kraehnert, R. Micelle-Templated Oxides and Carbonates of Zinc, Cobalt, and Aluminum and a Generalized Strategy for Their Synthesis. *Chem. Mater.* **2013**, *25*, 2749−2758.

(28) Ortel, E.; Reier, T.; Strasser, P.; Kraehnert, R. Mesoporous IrO_2 Films Templated by PEO-PB-PEO Block-Copolymers: Self-Assembly, Crystallization Behavior, and Electrocatalytic Performance. *Chem. Mater.* **2011**, *23*, 3201−3209.

(29) Agirrezabal-Telleria, I.; Hemmann, F.; Jäger, C.; Arias, P. L.; Kemnitz, E. Functionalized Partially Hydroxylated MgF_2 as Catalysts for the Dehydration of D-Xylose to Furfural. *J. Catal.* **2013**, *305*, 81−91.

(30) Landau, L.; Levich, B. Dragging of a Liquid by a Moving Plate. *Acta Physicochimica U.R.S.S.* **1942**, *XVII*, 42−54.

(31) Brinker, C. J.; Frye, G. C.; Hurd, A. J.; Ashley, C. S. Fundamentals of Sol−Gel Dip Coating. *Thin Solid Films* **1991**, *201*, 97−108.

(32) Faustini, M.; Louis, B.; Albouy, P. A.; Kuemmel, M.; Grosso, D. Preparation of Sol−Gel Films by Dip-Coating in Extreme Conditions. *J. Phys. Chem. C* **2010**, *114*, 7637−7645.